THE MINERALOGICAL MAGAZINE

AND

JOURNAL OF

THE MINERALOGICAL SOCIETY

No. 168 March, 1940 Vol. XXV

The Boxhole meteoritic iron, Central Australia.

(With Plates XX and XXI.)

By C. T. Madigan, M.A., D.Sc., B.E., F.G.S.

With chemical analysis by A. R. Alderman, M.Sc., Ph.D., F.G.S.

Department of Geology, University of Adelaide.

[Read November 9, 1939.]

THE Boxhole meteorite crater has been described previously.[1] It is in Central Australia at latitude 22° 37′ 30″ S., longitude 135° 11′ 59″ E. During the single afternoon that was spent examining this great crater, nearly 200 yards across, most of the time was occupied with taking measurements and photographs, and only a few shale-balls were found in the way of meteoritic material. Mr. Joe Webb, who lives nearby, was instructed to continue the search, and in due course he sent down to Adelaide three pieces of iron weighing respectively 17 lb. 9 oz., 1 lb. 8 oz., and 5 oz., shown in figs. 1 and 3, together with six more shale-balls. This material was purchased by the South Australian Museum. Two other small pieces of iron have been obtained by the author from other sources.

Mr. Webb said he found all the iron 150 yards from the east side of the crater, and the other two pieces were also said to have come from the east side. The iron fragments and shale-balls are in appearance indistinguishable from the Henbury specimens as figured by Dr. Alderman.[2] The largest piece, shown in text-fig. 1, has the typical appearance of any small iron meteorite that has undergone considerable weathering,

[1] C. T. Madigan, The Boxhole crater and the Huckitta meteorite (Central Australia). Trans. Roy. Soc. South Australia, 1937, vol. 61, pp. 187–190. [M.A. 7-12.]

[2] A. R. Alderman, The Henbury (Central Australia) meteoric iron. Rec. South Australian Museum, 1932, vol. 4, pp. 555–563. [M.A. 5-159.]

with its thumb-marks, smaller pitting, and dark-brown colour. It may well have been a separate member of a shower. There is no evidence of great strain or shattering, even in the polished section. The smaller pieces lack both the thumb-marks and small pitting. One of them, on the left in pl. xx, fig. 3, is equidimensional with concave depressions, two others are flat and dish-shaped, while the last, weighing 1½ lb. and seen on the right in fig. 3, is definitely torn and twisted, just like some of the Henbury fragments. The same suggestion presents itself as in the case of Henbury and Canyon Diablo, that some of the pieces of iron found near the crater are fragments of the exploded mass that formed the crater, and others are separate bodies that accompanied the main mass and fell as a shower. As the fragments seem to predominate on the eastern side, it would appear that the meteorite came from the east, the smaller members of the shower lagging behind.

The specific gravity was determined on the 17½ lb. piece of iron, by weighing in air and water, and was found to be 7·80.

The outer skin on the iron was not specially studied. It is merely a thin coating of oxide. Weathering has been considerable, shale-balls four inches thick being oxidized right through.

The iron cut comparatively easily with a hacksaw. A piece was cut off one end of the large specimen, near where the beginning of a saw cut can be seen to the right in fig. 1. The polished and etched section shows the structure of a medium octahedrite (pl. xx, fig. 4). The direction of section was not favourable to producing symmetrical figures. What is seen at a glance is bands of kamacite of comparatively uniform width, the average being 0·9 mm., running in four directions, a few well-defined and irregular cracks, which follow the kamacite bands and exude drops of hydrated lawrencite, and some scattered brassy grains of troilite. It is notable that the kamacite bands occupy almost the whole of the area, without enclosing any obvious fields of plessite. The longest continuous kamacite band is 16 mm. long. Most of the bands are in parallel sets from 4 to 8 mm. long. The troilite grains are mostly rounded, but two long narrow grains, each about 4 mm. long, were seen on the section. Other troilite grains are of the order of ½ to 1 mm. across.

A study of the surface under magnification shows several interesting features about the kamacite bands, and also the presence and nature of interstitial areas between the kamacite. The kamacite bands themselves are seen to be of two kinds. One, far the more plentiful, is made up of featureless grains of polygonal outline, bordered by straight to slightly curved cracks. This can be seen in pl. xxi, figs. 7 and 9, particu-

larly well. The other type of kamacite band, in some cases parallel and similar in dimensions to the common kind and in the same group with them, and in other cases more in the nature of interstitial areas between the normal kamacite bands, is made up of innumerable small laths of kamacite, with an infilling of taenite. In narrower bands of this type the laths are all parallel to each other and at right angles to the longer

FIG. 1. Meteoritic iron from the Boxhole meteorite crater, Central Australia. Weight 17½ lb. ×½.

side of the band; in broader areas the laths are at right angles to the margins all round. This is shown in fig. 5, where the large central grain is made up of laths normal to all its sides; while to the left centre a smaller area shows kamacite laths in two directions embedded in the black taenite, with a similar structure in the upper left. Fig. 6 shows six of these composite bands, all vertical, between the normal kamacite bands.

The kamacite bands are separated by a very thin bright line of taenite, which may thin out and disappear, leaving only a dark line. In other places the dividing line opens out and the taenite line divides and surrounds a minute dark area of plessite. The greatest width of plessite

is 0·2 mm. The bright taenite lines between kamacite bands are shown in figs. 8 and 10, with enclosed plessite. In some cases comparatively wide lines of taenite do not enclose plessite, as with the line appearing black at the top of fig. 5. Figs. 5 and 6 are microscope photographs in ordinary daylight. In them the black areas and lines are all composed of taenite. Figs. 7–10 were made with a metallography apparatus. In

FIG. 2. Shale-balls from the Boxhole meteorite crater, Central Australia. $\times \frac{1}{2}$.

them the taenite appears a clear white; also the images are reversed, left and right. The positions of the photographs are marked by the lettered circles on pl. xx. The area shown in fig. 7 lies inside that of fig. 5, and the central 'fish-shaped' area in fig. 5 appears near the bottom of fig. 7. The comparison is interesting, remembering that the figures are reversed, so that the 'fish' points in opposite directions. The taenite is black in fig. 5 and white in fig. 7. Fig. 7 shows that all the dividing lines between kamacite grains are not made up of taenite. Fig. 9 shows the interstitial taenite as composite grains and also some enclosed plessite in association with the taenite. Little rectangular areas of plessite like those shown are not uncommon, but they tend to be triangular and grade into the common narrow triangles which end the lines of taenite

between kamacite bands, as in figs. 8 and 10. The proportion of plessite is very low.

The shale-balls, of which some are shown in text-fig. 2, including the largest, do not call for special comment. They are quite similar to those from Henbury. They cannot be marked with a hacksaw, and seem somewhat siliceous, like the siliceous limonite form of gossan. The largest one was broken in two and was found to be oxidized completely through, with no core of iron. The shale is magnetic, crushes to a brown powder, and gives off water in a closed tube.

Dr. Alderman carried out an analysis of borings, taken from the surface left on the large piece from which the polished section was cut, with the following results (1):

	Fe.	Ni.	Co.	P.	S.	C.	SiO_2.	Total.
I.	91·77	7·80	0·44	0·08	0·03	0·049	0·01	100·18
II.	91·54	7·54	0·37	0·08	0·01	0·013	0·03	99·58

He says that, owing to the varying distribution of such minerals as troilite, the values given for sulphur, and probably phosphorus, may be taken as typical but not constant. The carbon was determined by Mr. T. W. Dalwood of the South Australian School of Mines assay department. The analysis is a normal one for iron meteorites of the medium octahedrite class, and shows no outstanding features. It compares very closely with Dr. Alderman's analysis (loc. cit.) of the Henbury iron, quoted under II.

It appears that all the large meteorite craters have been made by iron and not by stony meteorites, suggesting that the larger meteorites are all of iron, or perhaps that stony meteorites break up more readily in their passage through the earth's atmosphere.

In conclusion, it may be mentioned that a mass of 181 lb. (82 kg.) of the Boxhole iron was acquired in 1938 for the British Museum collection of meteorites [M.A. 7–73].

Description of Plates XX and XXI.

Meteoritic iron from the Boxhole meteorite crater, Central Australia.

(Photographs by H. E. E. Brock.)

Figs. 1 and 2 in the text.

Plate XX, Fig. 3. Two smaller pieces of Boxhole iron weighing 5 oz. (left) and 1 lb. 8 oz. (right). The right-hand piece is torn and twisted, indicating a fragment of the main disrupted mass. $\times \frac{1}{2}$.

Fig. 4. Polished and etched section of Boxhole iron. Kamacite bands running in four directions, cracks following the bands, and dark grains of troilite can be seen. Taenite does not show up, and plessite areas are too small to be distinguishable. The circles mark the areas of the enlargements in pl. xxi. $\times 2\frac{1}{2}$.

Plate XXI, Fig. 5. Composite grains or short bands of kamacite, consisting of short laths of kamacite at right angles to the sides of the grain, with a border of taenite (black) extending inwards between the laths. One such grain in the centre, one centre left, and one upper left. A wider streak of taenite is represented by the black line at the top. The remainder is kamacite as larger grains forming the normal bands. $\times 10$.

Fig. 6. Normal kamacite bands vertical and horizontal, with composite bands between. The latter are all vertical, three above, bordered by black lines of taenite, and three below, two of them much narrower. The black lines are taenite, the remainder kamacite. $\times 10$.

Fig. 7. A higher magnification of the central portion of fig. 5, with mirror image reversal. The borders of the kamacite bands and grains are clearly seen as dark lines, with a white line of taenite above, and the white interstitial taenite in the composite grains of kamacite. $\times 15$.

Fig. 8. A white line of taenite between kamacite bands, enclosing a triangle of plessite at one end. Composite grains are seen on the right. $\times 15$.

Fig. 9. Kamacite bands showing division into grains, and white taenite lines enclosing small dark plessite areas. $\times 15$.

Fig. 10. Taenite lines enclosing plessite between kamacite bands. $\times 15$.

Fig. 3

Fig. 4

C. T. Madigan: Boxhole Meteorite.

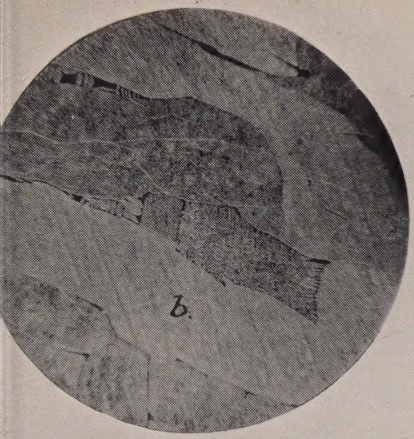

Fig. 5.

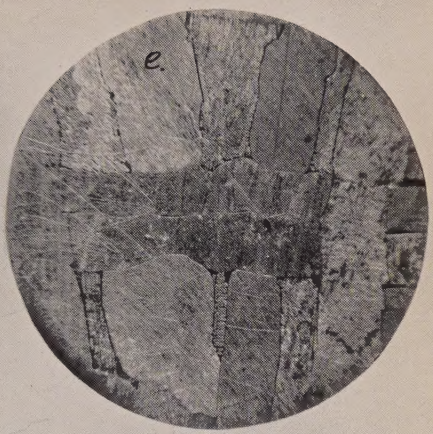

Fig. 6.

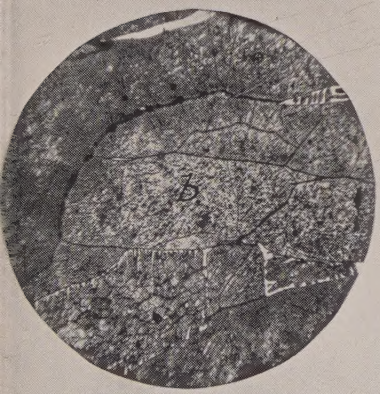

Fig. 7.

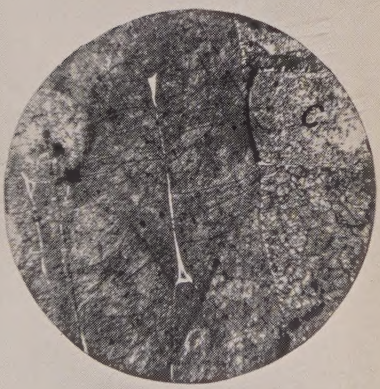

Fig. 8.

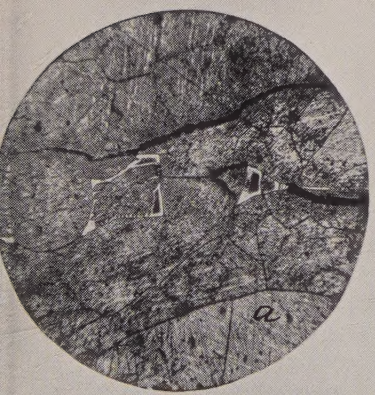

Fig. 9.

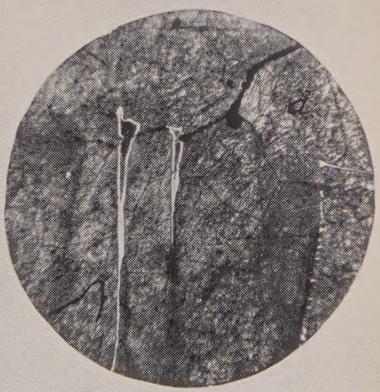

Fig. 10.

C. T. Madigan: Boxhole Meteorite.

Digitized by the Internet Archive
in 2023

https://archive.org/details/mineralogical-magazine_1940-03_25_168

Some australite structures and their origin.

(With Plate XXII.)

By George Baker, M.Sc.
Department of Geology, University of Melbourne.

[Read November 9, 1939; communicated by Dr. F. L. Stillwell.]

Introduction.

A NUMBER of specimens of core-like australites possess well-developed flaked equatorial zones (text-fig. 1), on which peculiar grooves and flutings are present. These markings are here referred to as 'bubble tracks', the term indicating their apparent mode of formation. The specimens displaying these features are round and elongate forms. The round forms vary in diameter from 34 to 41 mm., the elongate forms range in length from 30 to 75 mm., while the weights vary from 27½ to 96 grams. Australites of these sizes are of infrequent occurrence, only twenty-one having been previously recorded (9, pl. 4), (2, pl. 4), and (3, pl. 9); the illustrations of these examples show that they have comparable features, such as flaked equatorial zones and bubble tracks.

All of the specimens above referred to, and the features shown by them, suggest a mode of origin for core and bubble-track formation different from that of earlier explanations (3 and 4), which are based on the activity of superficial agencies operating on the earth's surface. The nature of the cores apparently substantiates a recently advanced hypothesis, in which core-like australites are thought to have been derived from spheres of australite glass by atmospheric flaking during flight (5, p. 202, fig. 2, stages 2 and 3); but an additional factor worthy of consideration is the effect upon the molten glass of hot gases accompanying the tektite during its pre-atmospheric stage of approach towards our planet (7).

Flaked equatorial zones.

The positions of the flaked equatorial zones on australite cores are diagrammatically represented in text-figs. 1A and 1B. These zones are

delimited from the posterior surfaces of the australites by sharply defined rims, towards which they invariably recurve outwards (pl. xxii). The flaked zones in some forms are broader than in others, being as much as 15 mm. in a specimen from Harrow, Victoria (fig. 4); the width

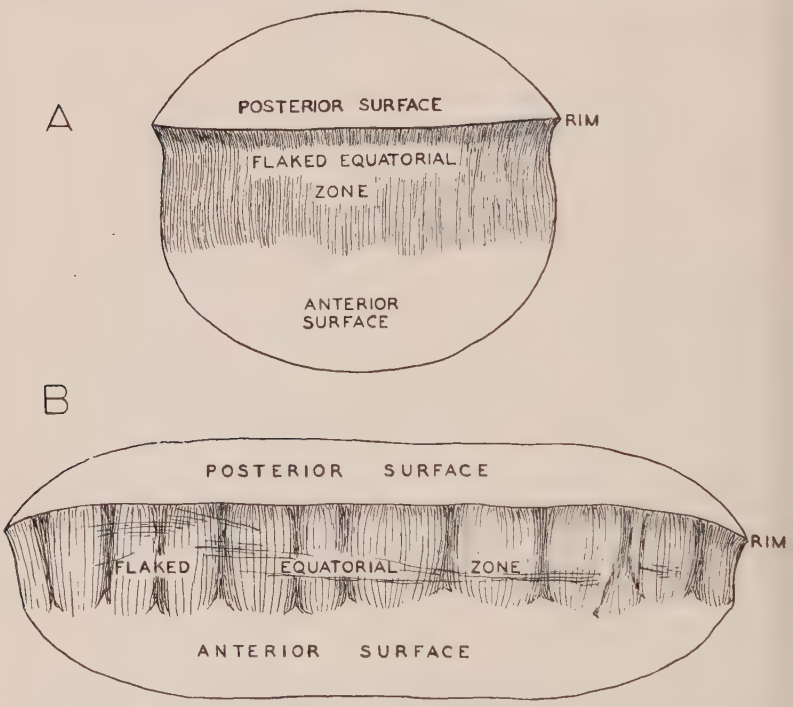

Fig. 1. Sketch diagrams of australite cores showing flaked equatorial zones.
A. Core of round form, illustrating recurving of flaked zone towards rim at junction with posterior surface.
B. Core of boat-shaped form. Darker shading represents ridges separating concave areas. Horizontal lines represent the more prominently developed flow-lines.

is more usually 8–10 mm. The zones are often marked with complex flow-line designs and occasional bubble pits (shallow depressions left on the surfaces of australites by escaping small gas bubbles), while bubble tracks often traverse the flaked zone parallel to the short axis of the australite (pl. xxii, figs. 1, 3, and 5).

The junction between the anterior surface and the flaked zone is occasionally pronounced and rim-like (figs. 3 and 8), but is never as sharply defined as the junction between the posterior surface and the

laked zone. Specimens such as this have two rims developed by flaking, he position of the well-defined posterior one being controlled by the nitial position of the original rim (produced by rotation during flight), he poorly marked anterior one arising essentially from the removal (see ater) of equatorial portions during flight. In most examples the nterior surfaces and the flaked zones merge imperceptibly into one nother, without any marked signs of the formation of a second rim figs. 4, 5, and 10).

The flaked zone of a boat-shaped australite from Port Campbell, Victoria (1, p. 169), is the best developed of any of the specimens xamined, and is apparently totally unaffected by agents of erosion fig. 9). Twenty depressed areas around this zone alternate with narrow idge-like portions arranged parallel to the short axis of the form. Bubble tracks are usually confined to these ridges, while fine flow-lines re more common on the surfaces of the depressions than on the ridges. Short grooves on the unflaked portions of the anterior surface occur at he anterior ends of the ridges and at right angles to them.

The flaking of equatorial regions in the larger australites has not esulted in the loss of much material from posterior surfaces. Practically l of the australite glass flaked away has been removed from the quatorial regions of the anterior surfaces. That the flaking ended arply at the posterior rim is indicated by a specimen from Caramut, ictoria (fig. 3), where seven-eighths of the periphery has been subjected flaking with the formation of a sharply defined rim; the remaining nflaked portion, at the right-hand end of fig. 3, shows remnants of the ss marked initial rim, continuous in position with the rim of the flaked ne.

There seems to be no doubt that these large australite cores have been oduced by natural means. The flaked zones do not resemble secon- rily chipped surfaces produced on australites by aboriginal flaking here the artificially flaked parts possess sharp ridges separating areas ith marked conchoidal and ripple fracture, but no flow-lines or bubble acks. Neither do they resemble the regions of flaking on smaller cores conical shape (3, pl. 4, figs. A1f, 7–12) which have no marked struc- res comparable to those on flaked zones of the larger cores. The flaked nes of the larger cores are too intimately associated with flow phe- mena to be adequately explained as due to agents such as abrasion, ., considered responsible for the production of the smaller cores p. 131, fig. 1).

The flaking process forming large australite cores seems best explained

by a cutting action due to the frictional resistance of the atmosphere against the australite during its earthward flight. The formation of the flaked zones around the periphery of the forward (anterior) surface was probably aided by a process of gas-bubble accumulation in the outer portions of the equatorial zones. As the region in which the bubbles collected would be rendered partially plastic and therefore less stable by secondary fusion brought about by atmospheric friction during flight, this collecting of bubbles of gas in the outer portions would further weaken the equatorial zones and make them more susceptible to atmospheric ablation. Remnants of areas in which bubble collecting occurred are indicated in fig. 5, where numerous bubble tracks lead to a large bubble crater (a cavity produced by the collapse of a large gas bubble) on the posterior surface. The numerous bubble pits, flow-lines, flow-grooves, and bubble tracks on the anterior side of the equatorial region of the only unflaked form amongst the larger australites examined (fig. 2) probably represent an early stage in gas-bubble accumulation prior to flaking. The apparent development of an initial flaked equatorial zone is shown in the photograph of this specimen; at each end there appears to be a modified area suggestive of flaking. Such a zone as this, on being further riddled with bubble pits and bubble tracks, would be more readily removed by atmospheric carving during flight than would the denser portions comprising the bulk of the australite; with the removal of this weakened zone, a pronounced flaked equatorial zone, and hence a core-like australite, would be produced.

Portions carved away from the periphery in this manner would be honeycombed with gas bubbles and would most likely be completely consumed during flight. Any less gassy portions flaked off might possibly constitute the initial forms from which small disk- and plate-like australites developed. Evidence probably supporting this suggestion is forthcoming from Port Campbell, Victoria, where certain australite fragments apparently fell to the earth independently of the larger parent form undergoing flaking. During their separate flight they commenced to form small irregular fragments, and assumed shapes somewhat comparable to the more perfectly developed disk- and plate-shaped australites.

Bubble tracks.

Grooves and flutings in flaked equatorial zones and on unflaked portions of the anterior surfaces of the larger forms of australites, are referred to as *bubble tracks* because in some examples they are chain-

ke arrangements of coalesced gas bubbles, often with vermicular segnented appearances (pl. XXII, fig. 1); in others the tracks are large ubble pits drawn out by the flowage of plastic australite glass. The ubble tracks are comparable with, but are neither as wide nor as deep s, grooves and flutings on certain forms of billitonites (8, p. 202). Flownes cutting the tracks at right angles to their length also intercept the m in parts of some examples, so that both the bubble tracks and the m were formed prior to the development of this particular set of flownes.

As regards the origin of bubble tracks, it has been suggested that mparable features referred to as grooves and flutings on other australes (4, p. 139) and on tektites in general (6, p. 64) are due to the emical corrosion of specimens which have been buried in moist soils r long periods, i.e. to partial solution by humic acids or alkalis in soils. his fails to explain the chain-like arrangement and segmented appearce of many of the bubble tracks. Moreover, at Port Campbell, ctoria, where the positions (i.e. as to which surface was uppermost) 388 australites were carefully noted at the time of discovery, it was and that flaked boat-shaped and round core-like forms with bubble cks occurred on similar soils close to other forms of australites which ow no such markings.

Since the bubble tracks fail to interrupt the sharply marked rims tween posterior surfaces and flaked zones and are never present on sterior surfaces, there is no reason to suppose that humic acids or kalis in soils should confine their activities to flaked zones and anterior rfaces, especially when it is the posterior surfaces which are invariably contact with the ground. This is the stable position of rest for australes, so that the posterior surfaces should be more prone to the suggested rrosion, as they were in contact with soils for longer periods than were terior surfaces; in fact, in several examples, the anterior surfaces may ver have been buried in soils, as the specimens may have rested on hard ound with their posterior surfaces downwards ever since they assumed eir stable position of rest after striking the surface of the earth. None the specimens so far examined ever show bubble-track markings on sterior surfaces.

An australite was immersed in concentrated hydrochloric acid for two nths, and an australite which had been ground and polished was mersed in concentrated potassium hydroxide for a similar period; at e end of this time no markings whatsoever had developed either on e natural or on the artificially prepared surfaces, whether in acid or

in alkali. This suggests that australite glass would be stable towards weak acids and alkalis in soils, and that it is homogeneous, so there is no reason for supposing that one part of an australite any more than another should be susceptible to corrosion whilst buried in moist soils. Linck has succeeded in corroding crystal-bearing tektites from Paucartambo in Peru by using hydrofluoric acid and sulphuric acid, and he thinks that similar etch marks could be caused naturally by corrosion of the tektite glass with hot accompanying gases or by the escape of these gases on the surfaces of the tektites (7, p. 231). He arrives at the conclusion that the origin of the sculpture of tektites cannot be due to etching by feeble corrosion whilst buried in the deposits in which they are found, as such corrosion would lead in the first place to hydration, and such a thing is never observed.

Moreover, it does not seem valid to interpret the bubble-track markings on australites as due to humic acids or alkalis in soils when bubble pits are regarded as original structures (3, p. 66). The markings are no more than grooves formed by chains of bubbles which have coalesced, or large elongated single bubbles, in all of the specimens containing them. When both are present bubble tracks and bubble pits are intimately associated on anterior surfaces and flaked zones, many of the tracks apparently starting or ending in pronounced pits or cavities; gas bubbles have fused together in an elaborate structure in much the same way as on other varieties of tektites (7, p. 231). The bubble tracks most likely resulted from the movement of lines of gas bubbles away from high-pressure regions (anterior surfaces) towards the equatorial regions against the resistance of the partially plastic australite glass. This process would occur partly during the phase of secondary fusion in the atmospheric stage of flight, but was probably initiated in the pre-atmospheric stage of the movement of these glass meteorites towards the earth, when strong corrosion may have been brought about by the action of hot accompanying gases.

Cores.

It is proposed that an australite *core* should be defined as 'the ultimate shape of any form of australite which has been reduced in size through loss of material from the periphery by a process of natural flaking. A pronounced flaked zone around the equator of the australite is produced by the action of terrestrial or atmospheric agencies, either on the earth's surface, or during flight'.

Such cores can be divided into three groups, according to their mode

f origin. First, there are the cores described as developing from regular utton-shaped australites from which the flanges were broken off after ll by abrasion, temperature variation, &c., after which further flaking ccurred around the equatorial zone (3, pp. 68 and 74). Many of the naller varieties of cores, 20 mm. and under in diameter, belong to this roup. Examples from Charlotte Waters in Central Australia and from ort Campbell, Victoria, have remnants of smooth bands, 2 mm. wide, dicating positions from which flanges have flaked away, and showing at the original unflaked forms were button-shaped australites. The aking away of these flanges apparently developed after the arrival of e australites at the earth's surface, as there has been no modification the original regions of flange attachment, such as would develop if aking had occurred during flight, when subsequent flowage would pro- ce secondary flow phenomena.

A second group of cores is made up of smaller round cores which show evidence that flanges have been flaked away from them. Such cores re probably developed from original lens forms (with rims) rather an from button forms (with flanges), probably in a manner analogous core formation from button-shaped australites.

The larger core-like australites with structures described above con- tute a third group of australite cores. In a recently elaborated theory, es (and the so-called bungs) similar to these are intermediate stages the evolution of round forms of australites (i.e. buttons and lenses, hich are round in posterior and anterior aspects) from original glass heres, by cracking and flaking off of unstable portions during atmo- heric flight (5, p. 202). The structures on such australites as those own in plate XXII and on those cores figured by Walcott (9), Dunn (2), d Fenner (3) are considered to substantiate this latest view of core rmation. Additional evidence for the possibility of such fragmenta- n occurring during flight has been indicated earlier (1, p. 175).

These three processes of core formation refer to round forms of stralites, but they are also applicable to elongate forms, since oval, at, dumb-bell, and teardrop-shaped australites may all possess flaked uatorial zones with markings comparable with those shown on round es.

Whether round or elongate in shape, none of these larger australite es constituting the third group appear to have been formed from nged australites, because large specimens with attached flanges have ver been recorded, and flange fragments of requisite size to suit these ger forms have never been found. Moreover, the larger australites

do not possess the flow-ridges so characteristically developed on the anterior (forward) surfaces of smaller forms (fig. 6). Presumably their anterior surfaces were insufficiently plastic for flowage to produce flow-ridges and ultimately flanges.

References.

1. Baker (G.) Tektites from the Sherbrook river district, east of Port Campbell, Victoria. Proc. Roy. Soc. Victoria, 1937, n. ser., vol. 49, pp. 165–177. [M.A. **7**–79.]
2. Dunn (E. J.) Australites. Bull. Geol. Surv. Victoria, 1912, no. 27.
3. Fenner (C.) Australites, Part I. Classification of the W. H. C. Shaw collection. Trans. Roy. Soc. South Australia, 1934, vol. 58, pp. 62–79. [M.A. **6**–18.]
4. —— Australites, Part II. Numbers, forms, distribution and origin. Ibid., 1935, vol. 59, pp. 125–140. [M.A. **6**–208.]
5. —— Australites, Part III. A contribution to the problem of the origin of tektites. Ibid., 1938, vol. 62, pp. 192–216. [M.A. **7**–276.]
6. Koomans (C. M.) On tektites and pseudo-tektites from Dutch East Indies and Philippines. Leidsche Geol. Mededeelingen, 1938, vol. 10, pp. 63–81. [M.A. **7**–275.]
7. Linck (G.) Oberfläche und Herkunft der meteorischen Gläser (Tektite). Neues Jahrbuch Min., Abt. A, 1928, Beil.-Bd. 57, pp. 223–236. [M.A. **3**–539.]
8. Merrill (G. P.) Handbook and descriptive catalogue of the meteorite collections in the United States National Museum. Bull. U.S. Nat. Mus., 1916, no. 94. [M.A. **1**–94.]
9. Walcott (R. H.) The occurrence of so-called obsidian bombs in Australia. Proc. Roy. Soc. Victoria, 1898, n. ser., vol. 11, pp. 23–53.

Description of Plate XXII.

Australites showing the core-like nature of some larger forms, with flaked equatorial zones and bubble tracks.

Photographs, natural size, by J. Spencer Mann. Posterior surfaces are uppermost in each photograph. Figures in brackets refer to the register numbers in the Melbourne University collection.

Fig. 1. Boat-shaped core. Kaniva, Victoria. (3045.)
Fig. 2. Unflaked boat-shaped form. Corop, Victoria. (3046.)
Fig. 3. Oval-shaped core showing unflaked remnant at right-hand end. Caramut, Victoria. (3099.)
Fig. 4. Core of round form. Harrow, Victoria. (2539.)
Fig. 5. Boat-shaped core with large bubble crater on posterior surface, to which numerous bubble tracks lead. Ellerslie, Victoria. (2572.)
Fig. 6. Button-shaped australite showing flow-ridges on anterior surface, and flange. Inverell, New South Wales. (3101.)
Fig. 7. Abraded core of round form. Harrow, Victoria. (2540.)
Fig. 8. Oval-shaped core. Ellerslie, Victoria. (2573.)
Fig. 9. Boat-shaped core with perfectly developed flaked equatorial zone and bubble tracks. Port Campbell, Victoria. (2970.)
Fig. 10. Abraded core of round form. Kalgoorlie, Western Australia. (3100.)

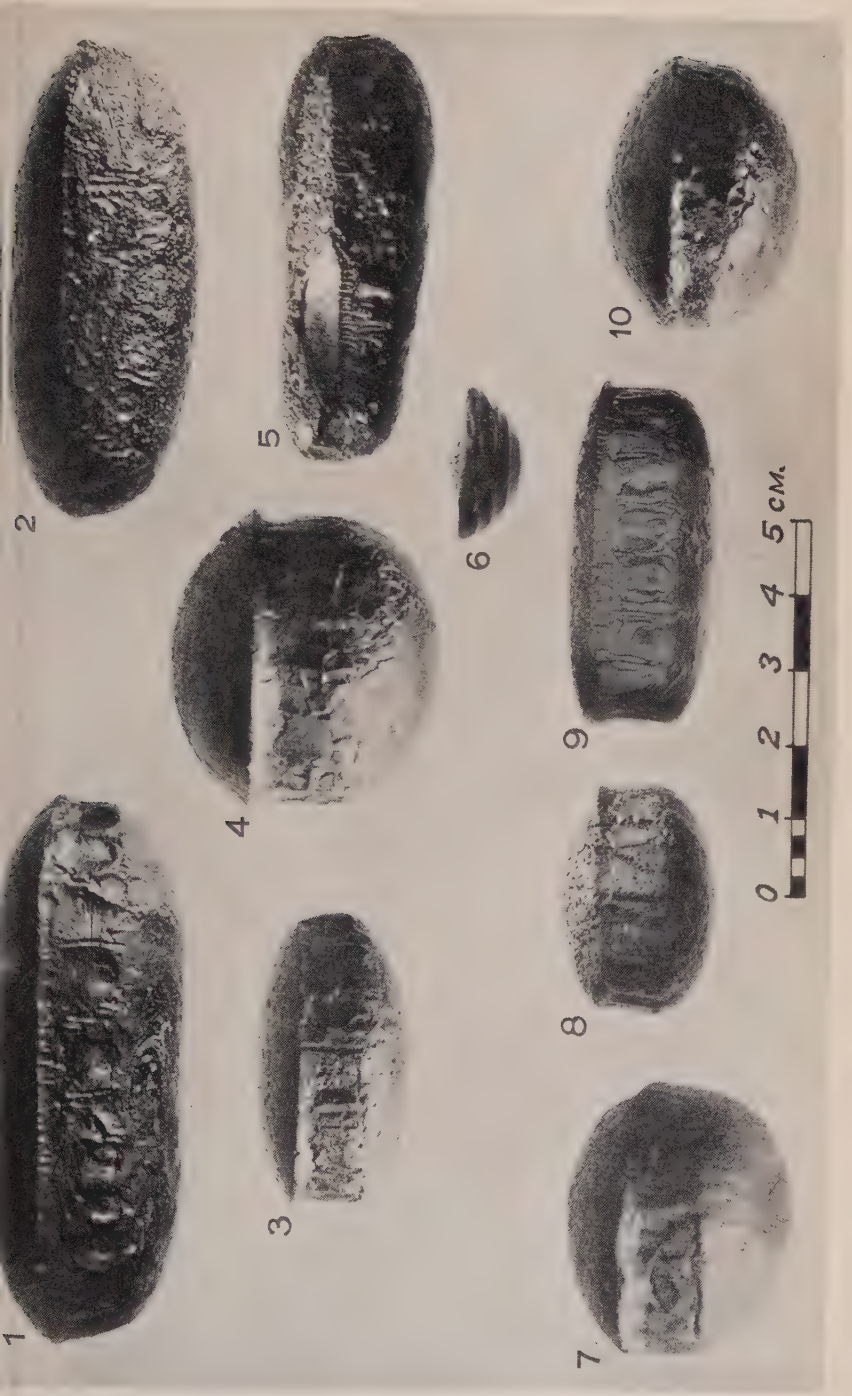

G. BAKER: AUSTRALITES.

Occurrences of bavenite in Switzerland.

By G. F. Claringbull, B.Sc., Ph.D., F.G.S.
Assistant-Keeper in the Mineral Department of the British Museum

[Read January 26, 1939.]

BAVENITE was first described from Baveno by Artini[1] in 1901 as monoclinic crystals of prismatic habit in pegmatitic druses in granite and given the formula $3CaO.Al_2O_3.6SiO_2.H_2O$. More recently, the mineral has been described pseudomorphous after beryl from Himalaya mine, Mesa Grande, San Diego County, California, by Schaller and Fairchild[2] (1932) and shown to contain beryllium as an essential constituent. In 1933 X-ray determinations by Ksanda and Merwin[3] indicated a unit cell with dimensions a 9·67, b 11·53, c 4·95Å., and showed the symmetry to be orthorhombic and referable to the space-group C_s^1, V_h^1, or C_{2v}^1. Revised crystallographic orientation and optical constants were also suggested by these authors.

The material about to be described is from two localities in Switzerland. Of fourteen specimens from a fissure in the rocks below the Muotta Nera, Piz del Laiblau, Val Nalps, Tavetschthal, Graubünden, selected by Mr. F. N. Ashcroft in 1935 and 1936 from a fairly large series stocked by Adolf Caveng of Sedrun, one (B.M. 1937,598) carries the mineral as roughly radiating aggregates of platy fibres of very pale brown colour in bulk. The largest mass measures about one cm. in diameter. Individual crystals from 0·01 to 0·05 mm. in width and rarely exceeding 2 mm. in length are colourless. No trace of the mineral has been found on the remaining thirteen specimens. Adularia, albite, sphene, epidote, quartz, chlorite, clinozoisite, and tremolite comprise the associated mineral assemblage of this fissure.

A further six specimens (B.M. 1939,592, 598, 602, 603, 605, 866) in a series of nineteen selected by Mr. Ashcroft in August 1938 from Caveng's stock have rounded brown masses of radiating crystals of bavenite of similar dimensions to those from Muotta Nera associated

[1] E. Artini, Atti (Rend.) Accad. Lincei, 1901, ser. 5, vol. 10, sem. 2, p. 139.
[2] W. T. Schaller and J. G. Fairchild, Amer. Min., 1932, vol. 17, p. 409. [M.A. 5–230.]
[3] C. J. Ksanda and H. E. Merwin, Amer. Min., 1933, vol. 18, p. 341. [M.A. 5–474.]

with albite, stilbite, apatite, adularia, and chlorite. With the exception of chlorite, which may clothe the bavenite aggregates with a thin green mantle of minute crystals, the beryllium mineral was the last to be deposited. The locality of these specimens is on the slopes of the east side of Val Casaccia, Val Cristallina, Graubünden.

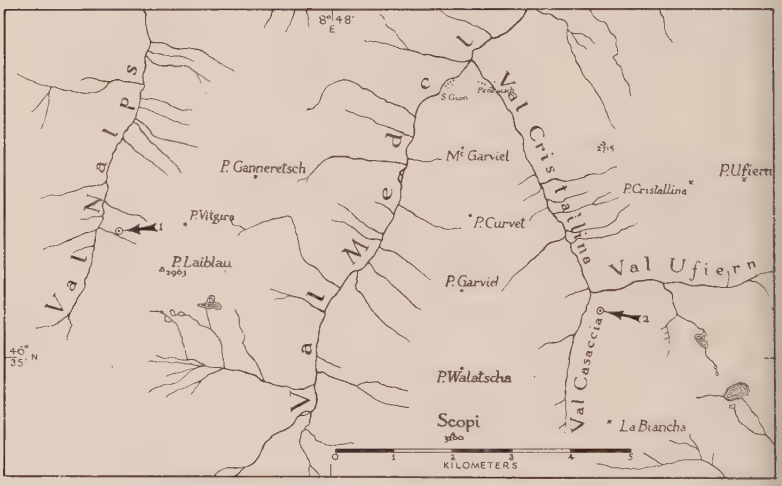

Fig. 1. Sketch-map of bavenite localities in Switzerland. 1, Muotta Nera. 2, Val Casaccia.

Assuming the orientation of Ksanda and Merwin, whereby the mineral is elongated parallel to [001] and the largest face becomes (010) making the cleavage parallel to (100), the Swiss crystals are striated parallel to [001] and no terminal faces have been observed. The refractive indices, α 1·583, β close to α, γ 1·589, and sp. gr. 2·74 are in good agreement with the published data.

The identity of the Swiss material has been demonstrated by comparison of a rotation photograph about the axis of elongation with a similar photograph of the mineral from the type locality. 10° oscillation photographs about each of three mutually perpendicular axes of rotation served to verify the orthorhombic character of the mineral and further gave cell dimensions of a 19·34, b 23·06, and c 4·95Å. The volume of the unit cell is thus four times that given by Ksanda and Merwin, and on the basis of 112 oxygen atoms and hydroxyl groups the unit-cell content is $Ca_{16}Si_{36}Al_8Be_4(O,OH)_{112}$, which may probably be grouped to the formula $4Ca_4(Si_9Al_2Be)O_{24}(OH)_4$.

Carbon are spectra of the type material from Baveno and that from
luotta Nera indicate the presence of similar quantities of beryllium in
ach. A series of comparison spectra of various silicon beryllium mix-
ures indicate that in both cases the beryllium exceeds one per cent. of
ie total. Besides the major constituents, boron occurs in both samples,
id its characteristic lines may also be observed in the published spec-
um of the Californian material. Magnesium and iron occur in small
nounts in the Muotta Nera bavenite and in less amount in that from
aveno. Germanium has been detected in the spectrum of the latter,
it not in that of the Swiss material.

The material described above is from a large collection of nearly
ven thousand precisely localized specimens of Swiss minerals presented
Mr. F. N. Ashcroft to the British Museum during the period 1921 to
39.

The writer is indebted to Dr. M. H. Hey who, on the basis of a pre-
minary optical examination and a microchemical test for beryllium,
ggested the identity of the mineral on the Muotta Nera specimen, and
Miss J. M. Sweet for directing his attention to the Val Casaccia
aterial.

The structure of orthoclase.

By S. H. Chao, A. Hargreaves, and W. H. Taylor,
Physics Department, College of Technology, Manchester.

[Read January 25, 1940.]

I. Introduction.

THE structure of sanidine was described by Taylor in 1933,[1] an Taylor, Darbyshire, and Strunz[2] in 1934 extended the investigatio to include the potassium-barium-felspars and albite, and presented small amount of experimental data for potash-soda perthitic felspar and for members of the plagioclase series. X-ray work on the potash soda perthitic felspars has recently been reported by Ito and Inuzuka, by Ito,[4] and by workers in this laboratory,[5] and a preliminary repor of an examination of the plagioclase felspars is given in a thesis presente by one of us (S.H.C.) in 1939 for the degree of Ph.D. in the Universit of Manchester.

The investigations to be described in this paper, as well as thos already published from this laboratory, form part of a programme o researches dealing with various aspects of the problem of felspa structure, undertaken in an attempt to obtain a correlation between th physical and chemical properties on the one hand and the details of th structure on the other. For this purpose it is essential that the 'key structures' of the felspar group shall be known as accurately as possibl The earlier work by Taylor and by Taylor, Darbyshire, and Strun included the determination, by *qualitative* methods only, of the structure of a specimen of sanidine of undetermined chemical composition, an of albite. If a structure is to be used as a standard of reference it desirable that *quantitative* X-ray methods shall be used, and that th

[1] W. H. Taylor, Zeits. Krist., 1933, vol. 85, p. 425. [M.A. **5**–473.]

[2] W. H. Taylor, J. A. Darbyshire, and H. Strunz, ibid., 1934, vol. 87, p. 46 [M.A. **6**–177.]

[3] T. Ito and H. Inuzuka, ibid., 1936, vol. 95, p. 404. [M.A. **7**–92.]

[4] T. Ito, ibid., 1938, vol. 100, p. 297. [M.A. **7**–396.]

[5] S. H. Chao, D. L. Smare, and W. H. Taylor, Min. Mag., 1939, vol. 25, p. 33 S. H. Chao and W. H. Taylor, Nature, 1939, vol. 143, p. 1024. [M.A. **7**–396.] S. H Chao and W. H. Taylor, Proc. Roy. Soc. London, Ser. A, 1940, vol. 174, p. 57.

hemical composition and physical properties of the specimen shall be nown. In this paper we describe our application of quantitative X-ray ıethods of measurement in the determination of the structure of a vpical orthoclase, containing only a small proportion of soda-felspar. 'he structure is, of course, similar in general features to that of sanidine, ut the details of the atomic arrangement can be given with much reater accuracy and certainty, and some interesting new features are evealed.

II. Experimental Details.

We have obtained all our experimental data from fragments of a ystal supplied by Dr. Edmondson Spencer, to whom we are indebted r much of the material which we have used in our researches. The resent material was collected by him at the ruby mines of Mogok in pper Burma, and was listed on the border-line of the moonstone and thoclase-microperthite series with the designation 'Specimen C, Burma lourless'. The chemical composition and physical properties given low are taken from his publications.[1]

The material contains 91 % (by weight) potash-felspar, 6·5 % soda-lspar, and 2·5 % lime-felspar; it is glass-clear and optically homo-eneous even under optimum illumination, and is free from schiller; e optic axial angle is 2V 44° in a plane perpendicular to the symmetry-ane and the extinction-angle on (010) is 5·3°. Spencer (1930, p. 330) ves reasons for supposing that the amount of soda-felspar (including me-felspar) actually present in this specimen may be held in solid lution, and we assume that our material represents a typical ortho-ase having the structure of pure potash-felspar.

To obtain Weissenberg photographs suitable for the quantitative easurement of intensities of reflection, crystal specimens of suitable mensions must be selected. The excellent (001) and (010) cleavages uplify the cutting of a needle-shaped fragment of uniform cross-ction and with its length parallel to the *a*-axis [100], but correspond-gly increase the difficulty of preparing a specimen of uniform section th its length parallel to *b* [010]. The fragments finally chosen were of mensions $1{\cdot}23\times0{\cdot}20\times0{\cdot}18$ mm. (length along *a* [100]), and $0{\cdot}6\times0{\cdot}2\times$ 2 mm. approximately (length along *b* [010]). The linear absorption efficient calculated for the Mo-Kα radiation (wave-length λ 0·71 Å.) ed in these experiments and for pure potash-felspar is 14, and refer-ce to Bradley's tables[2] for absorption corrections shows that for a

[1] E. Spencer, Min. Mag., 1930, vol. 22, p. 330; 1937, vol. 24, p. 465, pl. XVIII.

[2] A. J. Bradley, Proc. Phys. Soc. London, 1935, vol. 47, p. 879. [M.A. 6–164.]

cylindrical specimen of diameter 0·2 mm. the variation in absorption for the range of glancing-angles used is less than 1 %; for a specimen with *square* cross-section the maximum variation in absorption of reflections issuing in different directions in a plane normal to the needle-axis is not greater than 8 %, and for most reflections the uncertainty introduced by this factor will not exceed 4 or 5 %.

In an attempt to estimate the effect of extinction in reducing the measured intensities of the strongest reflections, a Weissenberg photograph was obtained from a fragment of crystal of dimensions 0·67 × 0·08 × 0·04 mm., with rotation about the needle-axis which is parallel to *a* [100]. The extinction correction will be discussed later.

The measurements previously reported (Chao, Smare, and Taylor 1939) show that the X-ray reflections confirm the monoclinic symmetry of the specimen and gave the following values for the axial lengths: *a* 8·60, *b* 13·02, *c* 7·22 Å. The angle β is assumed to have the value 63° 57′. If the crystal is assumed to be holohedral (a test for pyroelectric effect, using the liquid-air method, gave negative results), the space-group is $C_{2h}^3 = C2/m$. The unit cell contains four felspar molecules, the density calculated on the assumption that the crystal is a pure potash-felspar being 2·55, which compares sufficiently well with Spencer's measured density 2·563.

Reflections of the types (0*kl*) and (*h*0*l*) have been registered on zero layer-line Weissenberg photographs with crystal specimens (described above) rotating about the axes *a* [100] and *b* [010] respectively. The intensities of reflection have been measured by means of an integrating photometer of the Robinson-Dawton type,[1] due care being taken to obtain a reliable mean value of the integrated intensity for each reflection.

The most intense of all the reflections of the type (0*kl*) is the (002) and next in order are (040) and (060). Extinction is therefore most likely to affect (002), and we have attempted a very rough correction for this effect as follows. The smaller the fragment of crystal, the smaller is the influence of secondary extinction in reducing observed intensities below their true values. The use of a crystal of extremely small cross-section (0·08 × 0·04 mm.) should therefore result in relative enhancement of the strongest reflections if extinction is in fact effective in the larger specimen (section 0·20 × 0·18 mm.) from which the data for reflections (0*kl*) are obtained. Unfortunately, the *only* reflections of measurable intensity recorded on the film from the small crystal are (002), (040), and (060).

[1] B. W. Robinson, Journ. Sci. Instr., 1933, vol. 10, p. 233; and R. H. V. M. Dawton, ibid., 1937, vol. 14, p. 198.

) that it is impossible to make a thorough comparison of the alterations
1 relative intensities of very intense and of moderately weak reflections.
'he (002) is, however, relatively much stronger, compared with (040)
nd (060), when the small crystal is used, and an approximate correction
as therefore been applied to this one reflection.

For the reflections of type ($h0l$) no direct estimate of extinction effects
as attempted, owing to the difficulty of obtaining suitably shaped
)ecimens for rotation about b [010], but a correction was applied to
$20\bar{1}$), ($20\bar{2}$), ($20\bar{4}$), and (402), which are very intense reflections, the
nount of the correction being similar to that for (002).

The values of 'F_{observed}' quoted in table II include these corrections
or extinction. A few of the reflections included in the list of measured
's were too weak for photometric measurement and were estimated
isually; in the table these reflections are distinguished by the presence
f brackets—thus reflection (602), $F_{\text{obs.}} = (20)$.

To convert the integrated intensities of reflection, which are measured
on an arbitrary scale, into absolute F-values it is necessary to determine
least one integrated reflection in absolute units. This we were unable
o do, and we have therefore reduced our observed F's to an absolute
ale indirectly as follows. From the first synthesis of the projection
long the a-axis [100] approximate values of the atomic co-ordinates
and θ_3 can be deduced, and from these the F's were calculated for
reflections ($0kl$) which are neither very strong nor very weak. All the
easured F's for reflections ($0kl$) are now multiplied by that factor which
ecures the closest possible agreement between observation and calcula-
on for these reflections of medium intensity, and it is assumed that the
ew values of F ($0kl$) (observed) are now expressed in absolute units.
this comparison the very strong reflections are omitted because of
e uncertainty with regard to the effect of extinction, and the very
eak because of the difficulty of accurate measurement and the rela-
vely large effect of small changes in atomic co-ordinates.

To convert to absolute units the measured F's for reflections ($h0l$), the
bitrary scale of values is multiplied by a factor which makes the
tensities of reflections ($00l$) as measured on the film with rotation
out b [010] identical with the intensities of the same reflections as
easured on the film with rotation about a [100]. (The reflections ($00l$)
e, of course, the only set to appear on *both* films.)

It is clear that, although the measurements of F's are quantitative,
e final scale is not necessarily identical with the absolute scale. That
e scale of values quoted in table II is in fact identical with the absolute

scale to a very close approximation is shown, firstly, by the close agreement between observed and calculated F's for the structure as finally determined, and secondly, by the satisfactory agreement between the electron-counts in the projections obtained from the observed F-values and the known unit-cell contents (see section III).

Before the Fourier synthesis can be constructed from the measured F's it is necessary to know the sign of each F. For this purpose we have assumed that the structure of sanidine, as originally described by one of us (Taylor, 1933), provides a reasonably close approximation to the orthoclase structure now under discussion, and in the first synthesis for each axial projection the F's were given the same signs (+ or −) as for the sanidine structure. The F's were then recalculated using the atomic co-ordinates deduced from the first synthesis. Although many reflections show appreciable alterations in intensity, it is only in a very small number of the weaker reflections that there is a change of sign as compared with sanidine.

One further detail in the treatment of the experimental data must be described. The Fourier synthesis constructed from the measured F's is incomplete because no account can be taken of reflections at large glancing-angles which are too weak for measurement, which may nevertheless correspond to F's only *slightly* smaller than those which are included in the series. As a consequence, false detail may appear in the projection representing the Fourier synthesis. To remove this difficulty new syntheses were made, in which the coefficients were the F-values modified by the operation of an artificial temperature-factor of the usual form $e^{-B\sin^2\theta}$, where θ is the glancing-angle; with the value $B = 9$ the smallest coefficients are only a few units. In the resulting projections no false detail should appear.

III. Discussion of Results.

The orthoclase structure is very similar to that of sanidine, and reference should be made to the account (Taylor, 1933) of that structure for a description of its general features and for details of the space-group symmetry.

The results of our present measurements are summarized in the contoured graphs of electron-density reproduced in figs. 1A, 1B, 2A, 2B, which we now consider in turn.

Fig. 1A represents electron-densities projected along the b-axis [010] on the plane (010). The whole unit-cell area is included because otherwise it is difficult to see how the peaks lie in the cell. The quantity

hich is plotted is $S(xoz)$, the density per unit area being $S(xoz)/ac \sin \beta$, nd the contours drawn are $S = 0$ (dotted), 400, 1200, 2000, and at tervals of 800. Fig. 1B represents the corresponding projection, modi-ed by the application of the temperature-factor, as described in the revious section. The zero contour is again dotted, but contours are ow drawn, at uniform intervals of 400, for $S = 0$, 400, 800, &c.

Fig. 2A represents the projection, along the a-axis [100], of one-eighth the unit cell. The projection of the whole unit cell may be obtained y the operation of the symmetry elements, and the portion reproduced sufficient to enable the atomic peaks to be seen clearly. The quantity otted is $S(oyz)$, the density per unit area being $S(oyz)/bc \sin \beta$, and ntours are drawn at intervals of 400, the zero contour being dotted. ig. 2B is the corresponding projection when the artificial temperature-ctor is applied: the contours are 0 (chain-dotted), 200 (dotted), 400, 0, 1200 . . ., these being selected to give maximum clarity.

If all atoms were clearly resolved in both projections, it would be ssible to write down for each atom the co-ordinates θ_2 and θ_3 from e a-axis projection, and the co-ordinates θ_1 and θ_3 from the b-axis pro-ction; the two sets of values of θ_3 should be identical, and the agree-nt actually found would be a measure of the accuracy with which θ_2, and θ_3 have been determined for each atom.

In practice, as will be clear from figs. 1 and 2, there is serious over-pping of atomic peaks in many cases, and it is only by the use of both jections that any approach to a complete list of co-ordinates can be tained. The limits within which the atomic co-ordinates must lie, and eir most probable values, have been deduced from the projections: in me cases the range of possible values is small, in others it is rather rge; in many of the latter it has been possible to narrow the range direct comparison of observed and calculated F's for some reflection ich happens to be specially sensitive to a change in the particular -ordinate under consideration. Proceeding in this way 16 of the 20 riable parameters (co-ordinates) can be determined with considerable curacy, the remaining 4 being located within limits which correspond distances 0·1 Å., 0·2 Å. (for co-ordinates θ_3 of atoms O_B and O_C) and 2 Å., 0·3 Å. (for co-ordinates θ_1 of the same atoms). The final values these four atomic co-ordinates were selected in such a way as to make e tetrahedral $(Si,Al)O_4$ groups as regular in shape as possible: in doing is we are, of course, departing from the strictly impartial procedure ich was applied to determine the other 16 parameters, but we believe at we are justified, *firstly*, because there is a unique pair of positions

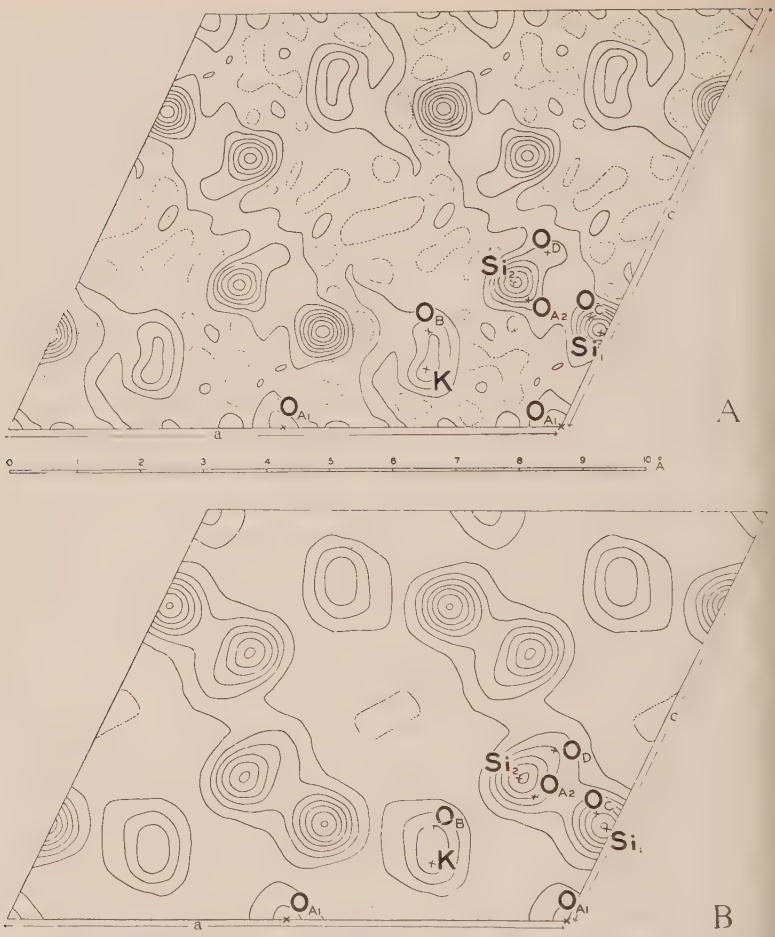

Fig. 1a. The electron-density projected along the *b*-axis [010]. The zero contour is dotted, and encloses regions of small negative density. The positions finally selected for the atoms are marked by crosses, which correspond to the co-ordinates quoted in table 1.

Fig. 1b. The electron-density projected along the *b*-axis [010] as in fig. 1a, the coefficients of the Fourier series being modified by the application of an artificial temperature-factor.

for O_B and O_C which results in almost perfectly regular tetrahedra about *both* atoms of types Si_1 and Si_2 (the co-ordinates θ_2 for both atoms being fixed in advance from consideration of the projections), and *secondly*, because the four co-ordinates finally chosen in this way (θ_1 and θ_3 for

O_B and O_C) all lie within the permissible limits previously established from the projections.

The atomic co-ordinates finally selected are shown in table I, which also contains the co-ordinates given in the sanidine paper (Taylor, 1933, p. 430.)

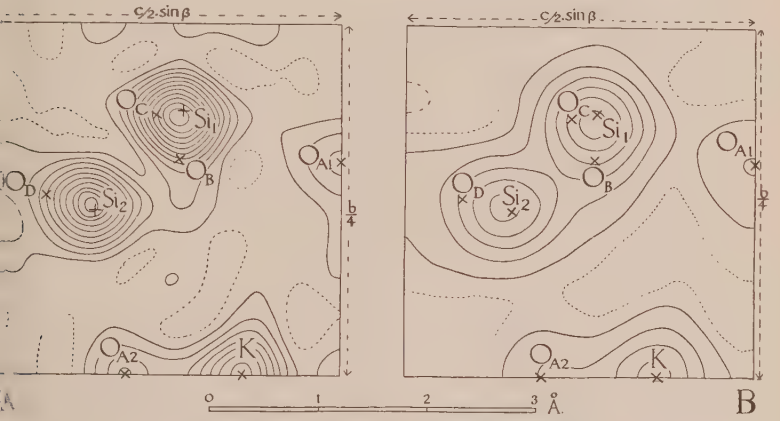

Fig. 2a. The electron-density projected along the a-axis [100]. The zero contour is dotted, and only one-eighth of the unit cell is shown in the diagram. Atomic positions represented by the co-ordinates quoted in table I are marked by crosses.

Fig. 2b. The electron-density projected as in fig. 2a, an artificial temperature-factor being included in the calculations. The zero contour is chain-dotted, and the 100 contour is dotted.

The accuracy of the structure represented by these atomic co-ordinates is confirmed if there is close agreement between the measured F's and those calculated from the structure for a large number of reflections of all types. Table II contains observed and calculated F's for reflections of types $(0kl)$ and $(h0l)$, and it is clear that there is very close agreement, with perhaps a slight tendency for $F_{calc.}$ to fall numerically below $F_{obs.}$. The weak reflections for which the intensity was estimated are marked by brackets in the column $F_{obs.}$, and the uncertainty as to the influence of extinction of the strongest reflections, and the accuracy of our corrections, must not be forgotten. Reflections are arranged in two sets, one $(00l)$ being included in both, corresponding to the photographs obtained by rotation about a and b axes respectively; in each set the reflections are in order of increasing glancing-angle. Fig. 3 presents the same figures in convenient graphical form. Since we are concerned to obtain high accuracy for a structure, the main features of which are

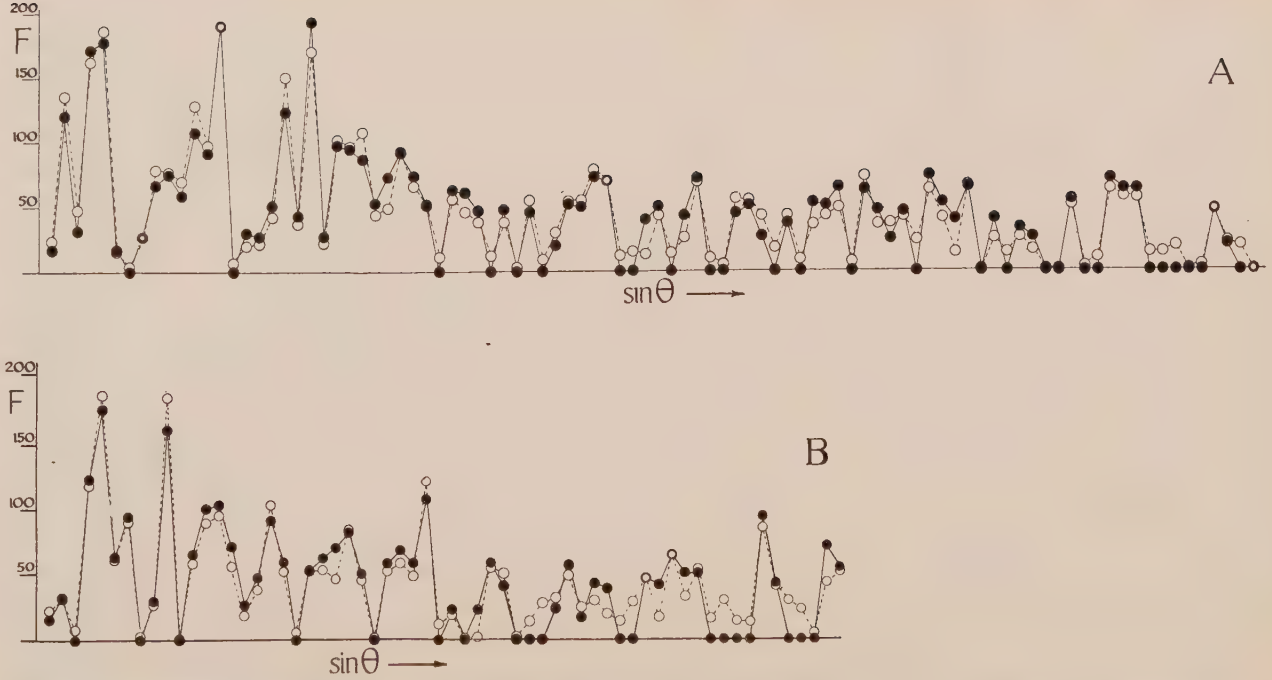

FIG. 3. Comparison of observed and calculated F's for reflections of the types ($h0l$) (fig. 3A), and ($0kl$) (fig. 3B). The reflections in each diagram are arranged in order of increasing glancing-angle, as in table II. Observed F's are represented by black circles connected by full lines, calculated F's by open circles connected by dotted lines.

TABLE I. Co-ordinates of atoms in the unit cell of orthoclase.

Atom.	Number in cell.	Orthoclase			Sanidine		
		θ_1.	θ_2.	θ_3.	θ_1.	θ_2.	θ_3.
O_{A1}	4	0°	55°	0°	0°	50°	0°
O_{A2}	4	240	0	109	237	0	85
O_B	8	295	55	82	295	55	85
O_C	8	15	114	94	0	115	90
O_D	8	62	46	150	55	45	150
Si_1	8	$3\frac{1}{2}$	$67\frac{1}{2}$	81	0	67	78
Si_2	8	$255\frac{1}{2}$	42	125	253	40	125
K	4	105	0	50	106	0	50

In the above table θ_1, θ_2, θ_3 are the angular co-ordinates defined by the expressions $\theta_1 = 360\frac{x}{a}°$, $\theta_2 = 360\frac{y}{b}°$, $\theta_3 = 360\frac{z}{c}°$, where x, y, z are the atomic co-ordinates in Å, and a, b, c are the axial lengths in Å.

For orthoclase the unit cell dimensions are a 8·60, b 13·02, c 7·22 Å., and the monoclinic angle β 63° 57′.

Silicon and aluminium are not distinguished in the above table. Reasons are given in section IV of the text for supposing that in orthoclase the group $8Si_1$ includes four silicon and four aluminium atoms, the group $8Si_2$ containing only silicon atoms.

The co-ordinates of the actual atoms marked by crosses in figs. 1 and 2 are all less than 180°. In some of the type-atoms included in the table the co-ordinate θ_1 is greater than 180°. In these cases the particular atom chosen as representing the group of 8 or 4 per unit cell, as the case may be, is selected to correspond with the atomic co-ordinates given in the original description (Taylor, 1933) of the sanidine structure, which are quoted alongside the orthoclase co-ordinates to facilitate comparison.

already known, it is not necessary to test reflections of the general type (hkl); this test was, of course, applied to the sanidine structure.

A further check on the accuracy of the work, and especially on the correct choice of the absolute scale of F-values, is obtained by counting electrons in the regions which represent atoms in the projections. In an ideal projection the background between atoms would correspond to zero electron-density, and the electrons could be counted for each of the clearly resolved atoms. In our projections there is much overlapping of atoms, and the background does not correspond to zero density; nevertheless, useful confirmation of the accuracy of the structure is obtained. For in *both* projections the total number of electrons per unit cell (including background) corresponds with the number of electrons in four molecules of $KAlSi_3O_8$, thus confirming that the scale of absolute units is correctly chosen (see section II). And the counts for separate peaks correspond approximately to the electrons in the atoms included in the peaks, as is shown in table III.

TABLE II. Comparison of observed and calculated F's for orthoclase.

(1) Reflections of the type ($h0l$).

Sin θ.	Indices.	$F_{obs.}$	$F_{calc.}$	Sin θ.	Indices.	$F_{obs.}$	$F_{calc.}$
0·055	(001)	16	$\overline{24}$	0·370	(80$\bar{6}$)	50	$\overline{43}$
0·083	(20$\bar{1}$)	121	136	0·373	(603)	0	14
0·090	(200)	32	$\overline{48}$	0·382	(007)	43	$\overline{28}$
0·107	(20$\bar{2}$)	172	$\overline{163}$	0·383	(206)	72	$\overline{69}$
0·110	(002)	178	$\overline{187}$	0·388	(405)	0	$\overline{10}$
0·122	(201)	17	16	0·390	(801)	0	$\bar{5}$
0·147	(20$\bar{3}$)	0	$\bar{4}$	0·395	(40$\bar{8}$)	45	56
0·164	(003)	27	27	0·400	(80$\bar{7}$)	51	$\overline{55}$
0·166	(40$\bar{1}$)	67	79	0·404	(60$\bar{8}$)	27	$\overline{43}$
0·167	(40$\bar{2}$)	75	77	0·411	(10.0.$\bar{4}$)	0	$\overline{18}$
0·169	(202)	59	70	0·412	(10.0.$\bar{3}$)	37	$\overline{43}$
0·182	(400)	108	129	0·417	(604)	0	9
0·184	(40$\bar{3}$)	92	$\overline{98}$	0·418	(10.0.$\bar{5}$)	53	36
0·196	(20$\bar{4}$)	191	191	0·419	(10.0.$\bar{2}$)	51	$\overline{43}$
0·213	(401)	0	$\bar{7}$	0·420	(802)	65	$\overline{49}$
0·216	(40$\bar{4}$)	30	$\overline{20}$	0·428	(207)	0	$\bar{7}$
0·219	(004)	27	21	0·431	(10.0.$\bar{6}$)	63	73
0·219	(203)	51	$\overline{42}$	0·432	(80$\bar{8}$)	47	36
0·247	(60$\bar{2}$)	124	$\overline{151}$	0·434	(10.0.$\bar{1}$)	25	37
0·247	(20$\bar{5}$)	43	37	0·438	(008)	44	42
0·250	(402)	194	$\overline{171}$	0·439	(406)	0	24
0·250	(603)	27	$\overline{22}$	0·445	(40$\bar{9}$)	74	63
0·266	(60$\bar{4}$)	98	102	0·448	(60$\bar{9}$)	53	41
0·269	(204)	95	97	0·451	(10.0.$\bar{7}$)	40	$\overline{14}$
0·273	(600)	87	108	0·454	(10.0.0)	65	66
0·274	(005)	52	44	0·458	(803)	0	$\bar{1}$
0·279	(60$\bar{1}$)	73	49	0·462	(605)	40	25
0·279	(40$\bar{5}$)	92	93	0·470	(80$\bar{9}$)	0	14
0·290	(60$\bar{5}$)	74	66	0·476	(10.0.$\bar{8}$)	33	$\overline{26}$
0·292	(403)	51	52	0·480	(10.0.1)	26	$\overline{16}$
0·299	(40$\bar{6}$)	0	$\overline{11}$	0·483	(208)	0	1
0·301	(20$\bar{6}$)	63	$\overline{56}$	0·489	(407)	0	$\bar{1}$
0·301	(601)	61	$\overline{46}$	0·493	(009)	55	51
0·323	(205)	47	38	0·495	(6.0.$\bar{10}$)	0	3
0·325	(60$\bar{6}$)	0	12	0·496	(4.0.$\bar{10}$)	0	$\overline{10}$
0·327	(80$\bar{3}$)	48	$\overline{38}$	0·498	(804)	71	63
0·328	(006)	0	$\bar{3}$	0·506	(10.0.$\bar{9}$)	63	57
0·331	(80$\bar{2}$)	46	55	0·509	(606)	63	$\overline{56}$
0·333	(80$\bar{4}$)	0	9	0·510	(10.0.2)	0	$\overline{14}$
0·335	(602)	(20)	30	0·536	(209)	0	$\overline{14}$
0·341	(404)	52	54	0·539	(10.0.$\bar{10}$)	0	$\overline{19}$
0·343	(80$\bar{1}$)	50	55	0·539	(805)	0	$\bar{1}$
0·346	(40$\bar{7}$)	73	$\overline{79}$	0·542	(408)	0	4
0·348	(80$\bar{5}$)	70	70	0·544	(6.0.$\bar{11}$)	47	$\overline{47}$
0·353	(20$\bar{7}$)	0	$\overline{12}$	0·545	(10.0.3)	(20)	22
0·362	(800)	0	$\overline{15}$	0·556	(607)	0	$\overline{19}$
0·362	(60$\bar{7}$)	40	$\overline{13}$	0·585	(806)	0	0

(2) Reflections of the type (0*kl*).

Sin θ.	Indices.	$F_{obs.}$	$F_{calc.}$	Sin θ.	Indices.	$F_{obs.}$	$F_{calc.}$
0·055	(001)	16	$\overline{24}$	0·319	(065)	(23)	19
0·055	(020)	32	$\overline{33}$	0·328	(006)	0	$\overline{3}$
0·077	(021)	0	8	0·328	(0.12.0)	(23)	2
0·109	(040)	124	$\overline{119}$	0·332	(0.12.1)	59	55
0·110	(002)	178	$\overline{187}$	0·333	(026)	(41)	51
0·122	(022)	64	62	0·343	(046)	0	$\overline{2}$
0·122	(041)	95	91	0·346	(0.12.2)	0	$\overline{14}$
0·155	(042)	0	$\overline{3}$	0·348	(0.10.4)	0	$\overline{28}$
0·164	(003)	27	27	0·350	(085)	(24)	$\overline{32}$
0·164	(060)	162	187	0·366	(0.12.3)	57	$\overline{49}$
0·171	(023)	0	$\overline{1}$	0·367	(066)	(17)	$\overline{25}$
0·173	(061)	66	59	0·382	(007)	43	$\overline{28}$
0·197	(043)	101	$\overline{90}$	0·382	(0.14.0)	(39)	$\overline{20}$
0·197	(062)	104	$\overline{96}$	0·385	(0.10.5)	0	$\overline{14}$
0·218	(080)	72	57	0·385	(0.14.1)	0	29
0·219	(004)	27	21	0·387	(027)	(47)	47
0·225	(081)	48	$\overline{39}$	0·393	(0.12.4)	(42)	17
0·226	(024)	92	$\overline{104}$	0·395	(086)	65	65
0·232	(063)	60	$\overline{53}$	0·397	(0.14.2)	(51)	33
0·244	(044)	0	$\overline{6}$	0·398	(047)	(51)	54
0·244	(082)	53	54	0·413	(067)	0	16
0·273	(064)	63	54	0·413	(0.14.3)	0	$\overline{30}$
0·273	(083)	71	47	0·425	(0.10.6)	0	14
0·273	(0.10.0)	83	85	0·425	(0.12.5)	0	$\overline{13}$
0·274	(005)	52	44	0·436	(0.16.0)	95	86
0·277	(0.10.1)	0	$\overline{1}$	0·438	(008)	44	42
0·279	(025)	59	$\overline{53}$	0·438	(087)	0	30
0·294	(0.10.2)	69	$\overline{59}$	0·438	(0.14.4)	0	$\overline{23}$
0·295	(045)	59	$\overline{49}$	0·438	(0.16.1)	0	$\overline{5}$
0·309	(084)	108	$\overline{122}$	0·449	(0.16.2)	(62)	$\overline{44}$
0·317	(0.10.3)	0	$\overline{12}$	0·493	(009)	55	51

The values of sin θ are for Mo-Kα radiation of wave-length λ 0·71 Å.

The reflections tabulated fall into two groups, with indices (referred to the crystallographic unit cell) of types (*h*0*l*) and (0*kl*) respectively; reflections (00*l*) occur in both groups, and are therefore included in both groups in the table. All reflections up to sin $\theta = 0{\cdot}4$ are included, but for larger glancing-angles only a selection of the possible reflections have been measured or been found definitely absent.

The column headed '$F_{obs.}$' contains *numerical* values of F in absolute units, the absolute scale being fixed indirectly as described in section II of the text. Values based on *estimated* intensities, where the reflections were too weak for photometric measurement, are enclosed in brackets ( ). The tabulated values for the reflections (20$\overline{1}$), (20$\overline{2}$), (002), (20$\overline{4}$), (402), are corrected for extinction as described in section II of the text. The value *zero* in this column indicates a reflection too weak for detection; the true value of the corresponding F is therefore appreciably smaller than the smallest value measured at glancing-angles of the same order of magnitude, but is not necessarily zero.

The calculated F's are for the structure represented by the atomic co-ordinates in table I. The atomic f-curves of W. L. Bragg and J. West (Zeits. Krist., 1928, vol. 69, p. 118. [M.A. 4–17.]) are used in the calculation.

TABLE III. Electron-counts from projections reproduced in figs. 1 and 2.

(1) Projection along *a* [100].

Atoms included in peak.	Number of electrons counted		Theoretical number of electrons	
	Fig. 2A.	Fig. 2B.	Neutral.	Ionized.
$Si_1+O_B+O_C$	25	27	29½	30
Si_2+O_D	20	24	22	20
O_{A1}	9	10	8	10
O_{A2}	7	7	8	10
K	17½	18	19	18
Total per unit cell	494	548	552	552

(2) Projection along *b* [010].

Atoms included in peak.	Number of electrons counted		Theoretical number of electrons	
	Fig. 1A.	Fig. 1B.	Neutral.	Ionized.
$2Si_1+2O_C$	40	40	43	40
$2Si_2+O_{A2}+2O_D$	46	49	52	50
$K+2O_B$	37	38	35	38
O_{A1}	10	10	8	10
Total per unit cell	532	548	552	552

In calculating the theoretical number of electrons for each peak, it is assumed that an atom Si_1 is equivalent to $\frac{1}{2}(Si+Al)$, for reasons given in section IV of the text. In the column headed 'Neutral' the atoms contribute the full number of electrons corresponding to the neutral atoms; in the column headed 'Ionized' it is assumed that the atoms are present in the form of the ions Si^{+4}, Al^{+3}, K^{+1}, O^{-2}.

If a count is made of the total number of electrons included in the background between the atomic peaks, the total number of electrons per unit cell, *including background*, is within a few units of the theoretical value 552. This indicates that the absolute scale of *F*'s is correctly chosen, as described in section III of the text.

In the projection along *a* [100] there is difficulty in drawing a distinct boundary between the first two groups of atoms, in both figs. (2A and 2B). In figs. 1B and 2B which correspond to the introduction of an artificial temperature-factor, the outlines of the peaks are very indefinite, and too much emphasis should not be laid on the very close agreement between the observed and calculated totals for the unit cell.

We may conclude that the details of the structure are correctly determined, and that the atomic co-ordinates quoted in table I are accurate within limits corresponding to shifts not exceeding ±0·1 Å., and probably smaller than this.

IV. FEATURES OF THE STRUCTURE.

The first question which arises in discussing the structure is its relationship with sanidine as described by one of us. The two structures are, of course, very similar—in fact, the sanidine structure was the starting-point for the present determination. Since the sanidine structure was determined by purely qualitative methods, there is no point in com

paring the precise details of the interatomic distances in the two structures: such a comparison will be of great interest when an accurate investigation of a sanidine is available, and this we hope to be able to provide in due course.

The dimensions of the tetrahedral groups in the orthoclase structure are as follows. In the tetrahedral group around atom Si_1 the silicon–oxygen distances are (in Å.) 1·66 to O_{A1}, 1·67 to O_D, 1·69 to O_C, 1·70 to O_B; and the oxygen–oxygen distances are 2·72 (O_{A1} to O_B), 2·72 (O_{A1} to O_D), 2·73 (O_C to O_D), 2·74 (O_B to O_D), 2·77 (O_{A1} to O_C), and 2·79 (O_B to O_C). In the group around Si_2, the silicon–oxygen distances are 1·57 to atoms O_{A2}, O_C, and O_D, and 1·60 to O_B; and the oxygen–oxygen distances are 2·51 (O_{A2} to O_D), 2·54 (O_B to O_C), 2·55 (O_B to O_D), 2·59 (O_{A2} to O_B), 2·59 (O_{A2} to O_C), and 2·65 (O_C to O_D). The difference between the two tetrahedra is very striking: the group around Si_1 is definitely, though of course only slightly, larger than the group around Si_2, with silicon–oxygen and oxygen–oxygen distances lying within the limits 1·66–1·70, 2·72–2·79 (for Si_1), and 1·57–1·60, 2·51–2·65 (for Si_2). Now the two groups of atoms '$8Si_1$' and '$8Si_2$' actually comprise 12 silicon and 4 aluminium atoms per unit cell (corresponding to 4 molecules of composition $KAlSi_3O_8$), and the obvious interpretation of the difference in the sizes of the two tetrahedral groups is that '$8Si_2$' includes only silicon atoms, whereas '$8Si_1$' includes 4 silicon and 4 aluminium atoms. The average size of the tetrahedron around Si_1 is increased because the (AlO_4) group is slightly larger than the (SiO_4) group, the four-co-ordinated aluminium ion being larger than silicon. It must be assumed that the distribution of aluminium atoms among the sites of the group '$8Si_1$' is random, since there is no evidence of any reduction of the symmetry from holohedry.

It will be extremely interesting to compare these tetrahedron dimensions with those of the corresponding groups in a specimen of the same material which has been heated for a long period at a temperature of about 1100° C., and so has suffered the structural change revealed by the permanent reduction of optic axial angle and its reversal into the symmetry-plane (Spencer, 1937, p. 476). It may be that the distribution of the aluminium ions among the tetrahedral groups is of primary importance in the process of 'sanidinization' revealed by the irreversible change in optic axial angle. We hope to investigate this problem.

The angles between bonds linking any given oxygen atom to two silicon (or aluminium) atoms are 147° (O_{A1} to Si_1 and Si_1), 152° (O_{A2} to Si_2 and Si_2), 152° (O_B to Si_1 and Si_2), 133° (O_C to Si_1 and Si_2), and 148°

(O_D to Si_1 and Si_2); these angles are probably accurate to within $\pm 5°$, and lie within the range of values usually observed in silicates.

The environment of the potassium atom is important for the comparison which will be made in the future with other structures containing sodium. The nearest neighbours are O_{A2} at 2·90, two O_{A1} at 3·00, two O_C at 3·09, two O_D at 3·11, and two O_B at 3·12 (all distances in Å.); the next nearest is another atom O_{A2} at 3·37 Å., but this is probably sufficiently distant to be excluded from the group of atoms which can properly be considered as in contact with the potassium ion. The potassium atom is thus surrounded by eight oxygen atoms at distances between 3·0 and 3·1 Å. (approximately), with a ninth atom (O_{A2}) at 2·9 Å., a group of the rather irregular type usually found around the larger cations in complex silicate structures.

One curious feature may be noted, though we are not sure whether it is of special significance. If our allocation of the aluminium atoms to the group Si_1 is correct, the oxygen atom O_{A2} is the *only* one to be linked to *two* silicon atoms (Si_2 and Si_2); for O_{A1} is linked to Si_1 and Si_1, and O_B, O_C, O_D to Si_1 and Si_2 (see preceding paragraph on bond-angles). The valency of the atom O_{A2} is therefore completely satisfied by its two silicon bonds, and we should expect to find no bond from O_{A2} to K. It is surprising to find that it is the nearest neighbour of the potassium atom, and it would appear that considerations of packing tetrahedra must outweigh the influence of the feeble bonds uniting monovalent potassium to the irregular group of oxygens around it.

The orthoclase structure described above is of value chiefly as a standard of comparison with structures of other felspars which we hope to be able to determine with comparable accuracy. In the meantime it is satisfactory to find that it fully confirms the essential accuracy of the felspar structures previously determined by qualitative methods.

V. Conclusion and Summary.

We have applied quantitative X-ray methods to the determination of the structure of a typical orthoclase containing nearly pure potash-felspar. The experimental procedure and the accuracy of the work are discussed, and the details of the structure are described.

We are indebted to Dr. Edmondson Spencer for the supply of material of known chemical composition. Two of us, S.H.C. and A.H., wish to express our indebtedness to the Government of Honan Province, China, and to the Manchester City Council, respectively, for the award of research scholarships which enabled us to undertake this work.